JACS
JOURNAL OF THE AMERICAN CHEMICAL SOCIETY
Article
pubs.acs.org/JACS

Oxidation of an Organic Adlayer: A Bird's Eye View

Thomas Waldmann,[†] Daniela Künzel,[‡] Harry E. Hoster,[†,§] Axel Groß,[‡] and R. Jürgen Behm*[,†]

[†]Institute of Surface Chemistry and Catalysis and [‡]Institute of Theoretical Chemistry, Ulm University, D-89069 Ulm, Germany

Supporting Information

ABSTRACT: The reaction of O_2 with an adlayer of the oligopyridine 2-phenyl-4,6-bis(6-(pyridine-2-yl)-4-(pyridine-4-yl)-pyridine-2-yl)pyrimidine (2,4′-BTP), adsorbed on the (111) surfaces of silver and gold and on HOPG − which can be considered as a model system for inorganiclorganic contacts − was investigated by fast scanning tunneling microscopy (video STM) and dispersion corrected density functional theory (DFT-D) calculations. Only on Ag(111), oxidation of the 2,4′-BTP adlayer was observed, which is related to the fact that under the experimental conditions O_2 adsorbs dissociatively on this surface leading to reactive O adatoms, but not on Au(111) or HOPG . There is a distinct regiospecifity of the oxidation reaction caused by intermolecular interactions. In addition, the oxidation leads to a chiral ordering. The relevance of these findings for reactions involving organic monolayers is discussed.

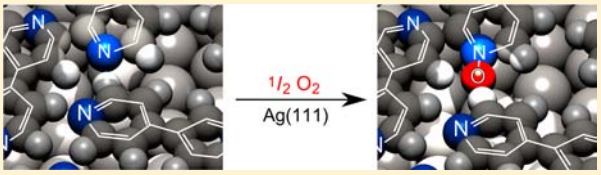

INTRODUCTION

Organic thin films and, ultimately, adsorbed monolayers (MLs) represent a class of new materials with interesting properties relevant for applications. These properties include nano-sized functionalities like molecular switches,[1] or transistors[2] which have mainly been explored by scanning probe techniques. In addition, organic MLs supported on conducting surfaces can serve as model systems for interfaces between organic regions and inorganic electrodes in macroscopic devices, such as OLEDs,[3−6] where charge is transferred at these interfaces, and thus, the operation properties of the devices are affected strongly by the interface properties. Chemical modifications of these contact regions by O_2 from the surrounding air, that can also diffuse through organic layers which are much thicker than a ML, can lead to aging and failure of a device.[4]

Studies of such reactions and in particular on the mechanism and kinetics of these processes, however, are scarce.[7−11] One reason for that is the generally very low concentration of reactive centers on the surface, which essentially precludes the detection and observation of these processes by standard spectroscopic surface techniques. This problem can be overcome by direct observation of the reaction process, using microscopy techniques.

Scanning tunneling microscopy (STM) has been successfully used for the observation of surface reactions or at least of the related structural changes on a molecular scale.[11−14] To the best of our knowledge, however, this technique has never been utilized to study the reaction of organic adlayers (or films) with small molecules present in the atmosphere with temporal resolution.

In this article, we report on the direct *in situ* STM observation of the reaction of an adlayer of large organic molecules, of an ordered two-dimensional (2D) phase of the oligopyridine 2,4′-BTP[15] (**1**, 2-phenyl-4,6-bis(6-(pyridine-2-yl)-4-(pyridine-4-yl)pyridine-2-yl)pyrimidine; see Figure 1) on Ag(111), with O_2 under ultrahigh vacuum (UHV) conditions.

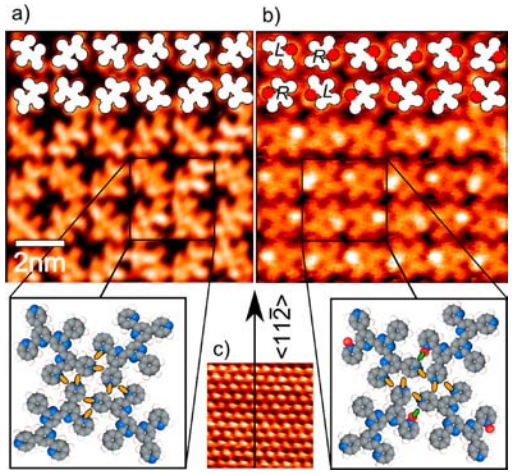

Figure 1. STM images (9.6 × 9.6 nm^2) of the α-phase prior to (a) and after (b) exposure to 1.3 × 10^{-5} mbar O_2 for 120 s. To guide the eye, footprint models of the molecules are superimposed in the top rows of both images. N···H−C interactions, orange colored; N−O···H−C, green. For larger area images see Supporting Information S1. (c) Atomic resolution (2.9 × 2.9 nm^2) of the clean Ag(111) surface with the sample in the same orientation as in panels a and b. Tunneling conditions: I_T = 40 pA, U_T = −2.20 V (a), I_T = 10 pA, U_T = −1.68 V (b), and I_T = 80 pA, U_T = −2.15 V (c).

For comparison, similar experiments were performed on Au(111) and HOPG substrates. Adlayers composed of **1** are particularly interesting because this molecule belongs to a group of pyridine derivatives with the same backbone (only the positions of the N atoms in the pyridne rings are different) that can be used as electron transport materials in highly efficient OLEDs, because of their ability to form hydrogen bonds.[5,6]

Received: September 2, 2011
Published: May 9, 2012

dx.doi.org/10.1021/ja302593v | J. Am. Chem. Soc. 2012, 134, 8817−8822

Thus, the well-known 2,4′-BTP adlayers[15−17] observed here can be used as a model system to study the reaction of an electrodel organic interface with O_2 on the molecular scale.

RESULTS AND DISCUSSION

Prior to the reaction, the surface is covered by a 2D ordered adlayer (Figure 1a), which is formed upon vapor deposition of ∼0.4 molecules nm^{-2}.[17,18] It results from weak N···H−C type hydrogen bonds (∼0.1 eV per bond) between the molecules,[15] in balance with localized vertical N···metal interactions.[17] This so-called α-phase was found to be the native structure of 2,4′-BTP formed on a variety of single crystalline surfaces at comparable coverage.[15,17−19] In the α-phase, the adsorbates **1** have azimuth angles (see Figure S3 in the Supporting Information) of ±15° with respect to the <11$\bar{2}$> direction of the Ag(111) and Au(111) surfaces (see Figure 1c for comparison with the atomically resolved structure of the clean Ag(111) surface) resulting in the same overlayer structure on both surfaces.[17,19]

Exposing the α-phase supported on Ag(111) to O_2 (1.3×10^{-5} mbar, 120 s, 298 K) leads to obvious modifications. While the overall structure and orientation of the adlayer is largely maintained, with the molecules essentially remaining at their sites, a more detailed inspection resolves local modifications of certain moieties in the individual BTP molecules (see Figure 1b, as well as S1 and Video 1 in the Supporting Information). Specifically, they develop a bright spot at the position of one of the peripheral 2-pyridyl groups (Figure 1b), which remains also after the O_2 exposure is turned off. A modification of the STM tip by an O atom as observed by Cheng et al.,[22] with both tip and sample at 5 K, is very unlikely in our measurements since (i) tip and sample are at 300 K, (ii) the structure of the α-phase on Au(111) and on HOPG did not change upon oxygen exposure, and (iii) imaging of the oxidized α-phase on Ag(111) did not change after voltage pulses of 10 V applied between tip and sample, which would have changed the tip configuration. Since the spots observed in our experiments were found to follow the movements of the admolecules in cases where the latter are locally mobile, these spots do indeed reflect modifications of the molecules and not of the underlying substrate (see Figure 2).

This kind of modification was observed upon O_2 exposure of the α-phase on Ag(111) and on the very similar (111) oriented Ag films[20] on Ru(0001), but not on Au(111) and HOPG (graphite). We note that bulk material of compound **1** is not even oxidized when exposed to air at a pressure 1 bar as shown previously by ^{1}H NMR, ^{13}C NMR, and mass spectrometry.[16] Since very thick layers are comparable to bulk material, we find a different reactivity for compound **1** than for observations on the oxidation of thicker pentacene films in organic transistors.[21] Instead, our results agree with a degradation mechanism in OLEDs where O_2 diffuses through thicker organic layers and oxidizes parts of the inorganiclorganic interface.

The chemical nature of the reaction products is not directly obvious. We tentatively associate the changes with N-oxide formation on the peripheral 2-pyridyl moieties, although direct proof is not possible from the STM images (see DFT calculations below). A closely related reaction involving adsorbed pyridine is the formation of pyridine N-oxides.[23] These species, which consist of upright standing pyridine rings bound to the surface via an oxygen atom, were found to form readily upon pyridine adsorption on oxygen precovered Cu surfaces.[23,24] The presence of the pyridine species on the surface was visible only indirectly, indicated by a change of the oxygen adlayer structure during *in situ* STM observation.[23] A similar interaction with oxygen covered metal surfaces was proposed also for other amines such as dimethylamine.[23]

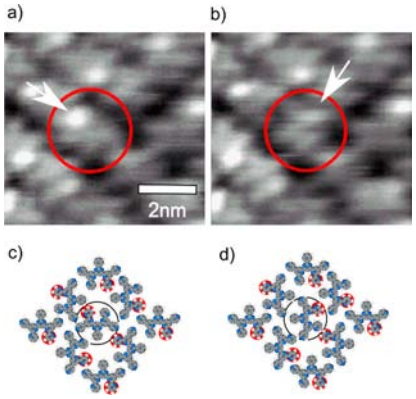

Figure 2. Type **2** molecule (large circle) switching between two orientations (a) and (b) and corresponding models (c) and (d). The bright spots (= 2-pyridyl rings) that are moving with the molecule are marked by arrows in panels a and b and by a red circle in panels c and d. Tunneling conditions: 1 frame s^{-1}, $p = 10^{-10}$ mbar, I_T = 158 pA, U_T = −2.25 V. The whole STM sequence can be found in video 1 of the Supporting Information.

The situation is different in our experiment, since the reacting pyridyl rings (see Scheme 1) are part of the flatly adsorbed molecules of type **1** in the ordered α-phase on Ag(111) (Figure 1a) which are exposed to O_2 gas, while in previous cases, ordered oxygen adlayers were exposed to gaseous pyridine or dimethylamine.[23,24] In analogy to the experiments on oxygen covered Cu surfaces,[23,24] a reaction following that in Scheme 1 is expected if adsorbed atomic oxygen (O_{ad}) is available on the surface. On Ag(111), this should be possible due to dissociative adsorption of O_2 from the gas phase.[25,26] Simulated STM images, comparable to STM images at negative bias (see Scheme 1, details of the DFT calculations are described in the Experimental Section), which also exhibit a characteristic 'protrusion' at the oxidized pyridine ring in product molecule **2**, further support this assignment. Finally, it is important to note that the STM data never showed an oxidized 4-pyridyl ring (configuration **4**), and a second

Scheme 1. Reaction of Adsorbed 2,4′-BTP (1) to Possible 2,4′-BTP N-Oxides 2−4 (here: R-form of 2 and 4) Catalyzed by Ag(111) at $p = 1.3 \times 10^{-5}$ mbar[a]

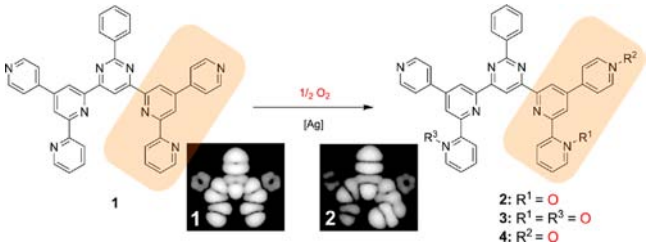

[a]The regions marked in orange correspond to the structures in Scheme 2. Insets show simulated STM images by summation of the two highest occupied molecular orbitals (HOMO and $HOMO_{-1}$) of the experimentally observed structures **1** and **2** at iso-values of 10^{-5} e/Å^3 (geometry optimization and energy calculations: B3LYP/TZVP with Gaussian03, planar molecules in gas phase).

dx.doi.org/10.1021/ja302593v | J. Am. Chem. Soc. 2012, 134, 8817−8822

oxidized 2-pyridyl ring (configuration **3**) was observed only in a few occasions (see inset in Supporting Information Figure S2d). Possible reasons for that will be discussed below.

The progress of the reaction was monitored in real-time by STM measurements with a frame rate of 1 s^{-1} (see Figure 3 and

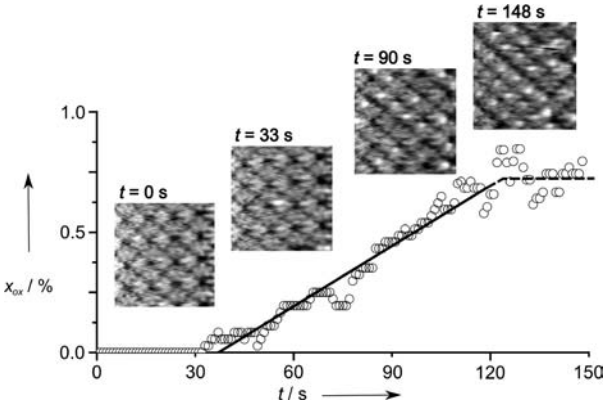

Figure 3. The fraction of oxidized 2,4′-BTP molecules x_{ox} as a function of time, as derived from a sequence of Video STM images (9.6 × 9.6 nm^2, 1 frame s^{-1},) recorded during exposure of the α-phase on an Ag(111) film to O_2 ($p = 1.3 \times 10^{-5}$ mbar). The plotted line shows the linear behavior indicating a 0th order reaction. The insets show typical STM images recorded during the transformation **1** → **2**. t = 0 s, α-phase ($p = 2 \times 10^{-10}$ mbar); t = 33 s, the leak-valve is opened ($p(O_2)$ = 1.3 × 10^{-5} mbar) and the first bright spot appears; t = 90 s, translational domains appear from one STM image to the other; t = 148 s, saturation (dashed line). The entire STM sequence can be found in video 2 of the Supporting Information. Tunneling conditions: I_T = 15.85 pA, U_T = −2.45 V.

video 2 in Supporting Information). This sequence of STM images shows directly that the orientation of the adlayer does not change during the reaction. The fraction x_{ox} of oxidized species relative to the total number of admolecules imaged, as obtained from counting in the sequence of STM images, is plotted as a function of time in Figure 3, together with some selected snapshots as insets. The data show an essentially constant increase of x_{ox} as a function of time until ∼72% of the admolecules are oxidized. The 'noise' in the data set is mainly due to a slight drift of the STM scan region, though there were few occasions (e.g., t = 49, 72, 73 or 77 s) where a bright spot disappeared again. It should be noted that STM images recorded in other areas of the sample (in the same experiment) revealed a slightly higher maximum yield of oxidized molecules (83 ± 6%). This indicates that the reaction itself is not induced by the STM tip. Instead, the actual local O_2 exposure might be reduced via shielding by the STM tip. Energetically, the incomplete oxidation of the organic adlayer may be related to the weakening of the hydrogen bonds due to the introduction of compressive stress (see below).

The linear slope of the increase of oxidized molecules corresponds to zero-order kinetics; the slope reflects a reaction rate of $r = (0.33 \pm 0.01) \times 10^{12}$ cm^{-2} s^{-1}. Considering the impingement rate Z of O_2 at 1.3 × 10^{-5} mbar and 298 K, calculated using kinetic gas theory

$$Z(O_2) \approx 2.63 \times 10^{22}\ \mathrm{cm^{-2}\ s^{-1}} \frac{p[\mathrm{mbar}]}{\sqrt{M[\mathrm{g\cdot mol^{-1}}]\cdot T[\mathrm{K}]}}$$

$$\approx 35 \times 10^{14}\ \mathrm{cm^{-2}\ s^{-1}}$$

and assuming that two molecules of type **1** are oxidized (two additional bright spots are created) by each reactively adsorbed O_2, we attain an initial reactive sticking coefficient of

$$S_0 = \frac{r}{2}\frac{1}{Z(O_2)} = (4.71 \pm 0.14) \times 10^{-5}$$

This value agrees reasonably well with the initial sticking coefficient reported for dissociative O_2 adsorption on clean Ag(111).[25] Since the Ag(111) surface is covered by a closed adlayer of the α-phase, dissociative O_2 adsorption must occur either at defect sites of the ordered adlayer, for example, at steps of the Ag substrate, or in the cavities of the α-phase. Dissociation at clean steps of Ag(111) is possible; however, the Ag steps are covered with **1**.[27] The dimensions of the cavities of approximately 0.78 nm × 0.45 nm[15,16] should be large enough to accommodate an adsorbing O_2 molecule (Figure 4b). The

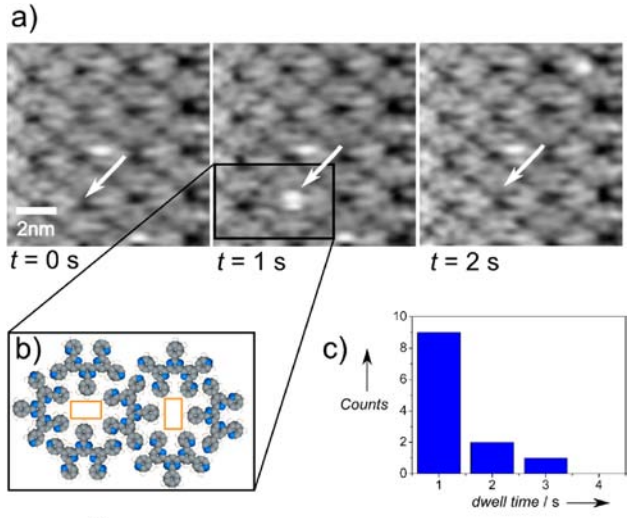

Figure 4. (a) Series of subsequent STM images showing bright spots inside the voids of the α-phase on Ag films with life times in the range of seconds (tunneling conditions: 9.6 × 9.6 nm^2, 1 frame s^{-1}, I_T = 15.85 pA, U_T = −2.45 V, $p = 1.3 \times 10^{-5}$ mbar O_2). (b) Model of the α-phase showing the voids with a size of ∼0.78 × 0.45 nm^2 (orange rectangles), where bare Ag(111) can be accessed by O_2. (c) Statistics of the lifetimes of O_2 in the voids of the α-phase on Ag films.

STM sequences obtained during O_2 exposure indeed resolved bright protrusions in some of the cavities, with an apparent mean lifetime of ∼1 s (Figure 4a,c). Neglecting the possibility of an abstraction mechanism for oxygen adsorption (see below), we tentatively assign these protrusions to a molecularly adsorbed O_2 precursor of O_{ad} formation. Since the lifetime is in the time scale required for a single STM image, we have to assume a considerable number of undetected events, so that we cannot quantitatively correlate the numbers of temporary protrusions (adsorbed O_2 precursors) and permanent spots (molecules of type **2**). It should be pointed out that the stable protrusions neither showed a preference for appearing in pairs nor for forming in the neighborhood of the temporary protrusions (see Video 2 in Supporting Information). In principle, this can be explained by two possibilities: either O_{ad} is highly mobile within the organic adlayer or O_{ad} is formed via abstraction from O_2, similar to the mechanism proposed for O_{ad} formation on Al(111).[28] We find the first model to be more likely. This is supported by the reaction kinetics: zeroth-order adsorption kinetics can be rationalized by a rate-limiting

dx.doi.org/10.1021/ja302593v | J. Am. Chem. Soc. 2012, 134, 8817−8822

dissociative adsorption step, followed by fast reaction with one of the adsorbed molecules. In that case, the number of O_2 accepting cavities remains constant. In contrast, for the abstraction mechanism, the number of reactive molecules decreases during reaction, which would point to first-order kinetics. Further evidence for a rate-limiting dissociative adsorption step comes from the calculations discussed below.

In addition to the adsorption kinetics, the STM data also resolve details on the spatial organization of the oxidized admolecules **2**. First of all, these form statistically on the surface; we have no indication for a reaction process proceeding via formation and 2D growth of islands. Second, detailed analysis of the STM images reveals a clear order of the chiral product molecules of type **2** in the α-phase. R- and L-version of the oxidized molecules, with O at the R_1 or R_3 position, respectively, arrange in a strict alternating order along the adlayer lattice orientations (see Figure 1b), with an enantiomeric excess of only ∼1.0% derived from more than 1700 molecules in the STM images, corresponding to a racemate. Possible origins will be discussed below.

The energetics of the proposed reaction were explored via dispersion corrected density functional theory (DFT-D)[29] calculations, using the smaller molecules **5** and **6** as models for reactant (**1**) and product (**2**) molecules, since the original molecules would have been computationally too expensive. The molecules **5** and **6** are parts of **1** and **2**, respectively, and can give useful trends regarding the reactivity in Scheme 1, though they do not provide exact values for the situation in the experiment. However, the reactive chemical moieties (pyridine-N groups) in **5** and **6** are very similar and thus comparable to those in **1** and **2** or other pyridyl compounds.[31]

Molecules **5** and **6** were considered adsorbed on Ag(111) and Au(111) (for adsorption geometry, see Scheme 2) and in the gas phase. With products and reactants in the gas phase, the reaction shown in Scheme 2 is exothermic by −0.62 eV. When **5** (reactant) is adsorbed on either Au(111) or Ag(111), its reaction toward the adsorbed species **6** is exothermic by −0.84 and −0.93 eV, respectively. Energetically, the reaction is thus less favorable on Au(111) than without a supporting surface, whereas on Ag(111), the product **6** is additionally stabilized. Apart from the energetic stabilization of the product, its formation is further facilitated by the lower dissociation barrier of O_2 on Ag(111) (∼1 eV[30]) as compared to Au(111) (∼2 eV[30]) which is, like HOPG, known to be inactive for O_2 dissociation.[25,26]

Scheme 2. Model for the Reaction Shown in Scheme 1[a]

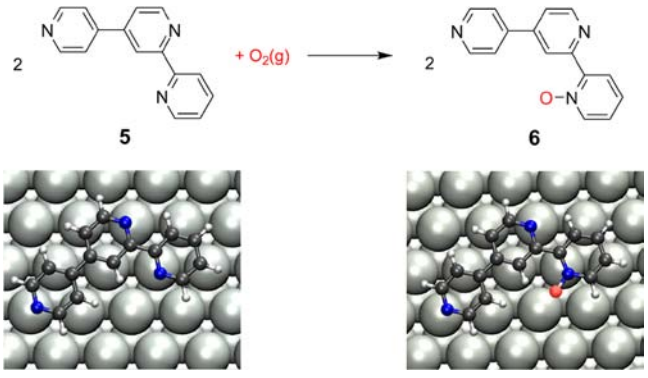

[a]Compare the marked regions in Scheme 1. In the DFT-D[29] calculations, **5** and **6** were considered in the gas phase and adsorbed on Ag(111) and Au(111). The insets show the adsorption geometries on Ag(111) (see text).

Having confirmed that the formation of an N-oxide at a peripheral pyridyl moiety is an energetically favorable process and that Ag catalyzes this process, the experimental data still leaves an open question. We only observe the formation of molecules **2**, while **3** is found rarely (inset of Supporting Information Figure S2d) and **4** is totally absent, though all pyridyl moieties should in principle be similarly reactive for N-oxide formation. This can be rationalized by looking at the molecule−molecule interactions before and after oxidation of the BTP adlayer. As shown in Figure 1 (see also Supporting Information, Figure S2), the oxidized pyridyl groups form N−O···H−C type hydrogen bonds with neighboring molecules.[31] The N−O bond length of ∼0.13 nm, however, is now introduced as additional "spacer", which compressively stresses the adlayer. Since a DFT-D description of four molecules of type **1** or **2** on three slabs of Ag would already consist of over 1500 atoms, it would be computationally much too expensive. To estimate the possible effect of the changed hydrogen bond configuration on the adlayer stability, the hydrogen binding interaction energy of the α-phase in the initial and oxidized state is estimated in a pairwise interaction model (∼0.1 eV per hydrogen bond),[15] in which the molecules are regarded as rigid objects in a 2D plane without a supporting surface. Using a Metropolis Monte Carlo algorithm and MP2 based, distance dependent C−H···H−C and N···H−C interaction energies,[15] the system configuration is varied until a minimum energy configuration is attained for molecules **1**−**4** (for details see Supporting Information Figure S2a).[17] By using periodic boundary conditions, the packing density of the molecules is fixed to the experimentally found value. The stability of an adlayer consisting of admolecules **2** (−0.44 eV per molecule, Supporting Information Figure S2c) is comparable to the one consisting of **1** (−0.47 eV, Supporting Information Figure S2b). In contrast, if each molecule in the α-phase consists of admolecules of type **3** (Supporting Information Figure S2b) or **4** (Supporting Information Figure S2e), the total hydrogen bond energies are only −0.38 eV and +0.18 eV (= destabilization) per molecule, respectively, in perfect agreement with the experimental findings (see above). Hence, the molecule−molecule interactions provide a clear energetic driving force for the observed regiospecifity of the oxidation reaction. Regarding the alternating occurrence of the L- and R-version of the oxidized molecule, our pairwise interaction model did not indicate a significant energetic effect of the lateral enantiomer distribution of **2** in the α-phase. Therefore, we tentatively assign the observed order to substrate registry effects, that is, to a better fit of the oxidized adlayer to the substrate lattice. Indeed, the DFT-D adsorption energies of **5** and **6** on Ag(111) tend into this direction. **5** has the same orientation with respect to the <11$\bar{2}$> direction of the Ag(111) surface as **1** in previous experimental studies.[17,19] This adsorption geometry, where all N atoms of **5** are near on-top positions with respect to the Ag atoms (see left-hand side of Scheme 2), is favored by ∼0.1 eV compared to that geometry where all N atoms are near the on 3-fold hollow sites of Ag(111) (adsorption energies 1.72 and 1.62 eV, respectively). Since the STM sequences in Figure 3 clearly demonstrate that the adsorbates do not change their orientations during the reaction, the adsorption energy of **6** should be also calculated in the orientation that is the best for **5**. This adsorption geometry,

dx.doi.org/10.1021/ja302593v | J. Am. Chem. Soc. 2012, 134, 8817−8822

where the N atoms of **6** are on-top of Ag atoms (right-hand side of Scheme 2), results in an adsorption energy of 1.83 eV. The fact, that this is not the lowest energy for **6** indicates an effect of the substrate, additional to the stress in the adlayer induced by the N−O spacer (see above).

In total, we could follow the spatial progress and unravel mechanistic details of the oxidation process of an organic monolayer film, of an ordered oligopyridine adlayer on Ag(111), upon exposure to O_2 under UHV conditions, by direct STM observation, dispersion corrected DFT calculations, and Monte Carlo simulations. Our findings point to a reaction mechanism proceeding via dissociative adsorption of O_2 in the cavities of the ordered phase, and subsequent reaction of the resulting O_{ad} species with the oligopyridine. Stress minimization has been identified as the driving force for the observed regiospecifity of the oxidation reaction, whereas the distribution of the resulting oxidized enantiomers is attributed to molecule−substrate interactions. The study reveals a distinct difference in reactivity of the organic monolayer with O_2 depending on the supporting surface. Similar reactions can in principle take place with other types of molecules and on other catalytically active surfaces. The sensitivity of the tested organic network to the reactive gas shows that in cases of similar reactivity, the inorganic/organic contacts in organic devices would have to be fabricated under high vacuum conditions and protected to avoid aging processes. On the other hand, similar reactions may lead to desired interface properties and the same principle may be useful for ultrasensitive gas sensors.

The approach described in this paper shows that surface reactions involving large adsorbates can be followed with ultimate sensitivity, reaching down to the single-molecule level, by using Video STM and that detailed, quantitative reaction data can be collected by statistic evaluation. This way, the method can gain insight into other surface catalytic systems or aging processes at electrode/organic interfaces which occur in organic devices or in batteries.

EXPERIMENTAL SECTION

The experiments were carried out in two standard UHV chambers with base pressures $<2 \times 10^{-10}$ mbar. Au(111) and Ag(111) single crystals were cleaned by Ar^+ sputtering and annealing to 770 K for 5 min. The fast STM measurements were conducted on an Ag thin film on Ru(0001). The Ru(0001)-surface was cleaned by repeated cycles of Ar^+ sputtering (0.5 keV, 4 μA, 30 min) and flash-annealing to 1650 K. Carbon impurities were removed by exposure to 10^{-6} mbar O_2 for 10 s, followed by flash annealing to 1650 K. Evaporation of 3 ML Ag and heating to 770 K for 4 min led to a surface similar to Ag(111).[20] The cleanliness of each surface was checked after all preparation steps by Auger electron spectroscopy (AES), STM, and low energy electron diffraction (LEED). **1** was deposited by a Knudsen-type evaporator, leading mainly to monolayers of the α-phase. STM and video-STM measurements made use of an Aarhus type variable temperature STM (SPECS) and a home-built 'pocket-size' Video STM, respectively. All STM experiments were done at room temperature and with W tips. Oxidation of the organic adlayer was attempted by exposure to 1.3×10^{-5} mbar of O_2 (99.998% purity) through a leak valve. STM images were recorded with voltages between −1.68 and −2.45 V, and tunneling currents were in the range of 10−40 pA.

The total hydrogen bond energies of the initial and the oxidized oligopyridine adlayers were calculated by summing over pairwise interaction energies. In analogy to the treatment in a previous study,[15] the interaction potentials were derived from MP2 calculations (Supporting Information Figure S2a).[17] Via periodic boundary conditions, the adlayer density was kept at the experimentally found value, but it was allowed to relax via lateral movements and rotations of the molecules according to a Metropolis Monte Carlo algorithm.[17]

STM simulations of the isolated oligopyridine molecule were based on B3LYP/TZVP;[32,33] calculations with Gaussian.[34] For the DFT optimization of the oxygen/terpyridine systems, on Ag(111) and Au(111), periodic DFT calculations with the PBE[35] functional were performed within a (5×7) geometry with 4 layers (topmost layer distance relaxed) using the VASP[36] code. Ionic cores were represented by the projector-augmented-wave (PAW) method.[37] For the sampling of the Brillouin zone, a $1 \times 1 \times 1$ k-point grid was employed. The one-particle states were expanded in a plane wave basis with an energy cutoff of 400 eV.[38] Dispersion correction was based on the DFT-D FORTRAN program by Grimme and co-workers.[29] We used our own implementation into the VASP code.

ASSOCIATED CONTENT

Supporting Information

Experimental and theoretical details, additional STM images and MC based calculations. This material is available free of charge via the Internet at http://pubs.acs.org.

AUTHOR INFORMATION

Corresponding Author

juergen.behm@uni-ulm.de

Present Address

[§]TUM CREATE Centre for Electromobility, 62 Nanyang Drive, Singapore.

Notes

The authors declare no competing financial interest.

ACKNOWLEDGMENTS

This work was supported by the Deutsche Forschungsgemeinschaft via the Collaborative Research Centre (SFB) 569 (Projects B11 and A7). T.W. acknowledges a fellowship by the Landesgraduiertenförderung Baden-Württemberg. We thank C. Meier, D. Caterbow and U. Ziener for providing the 2,4′-BTP material, M. Roos for help with the MC simulations and the bwGRiD[39] project for computational resources.

REFERENCES

(1) Auwärter, W.; Seufert, K.; Bischoff, F.; Ecija, D.; Vijayaraghavan, S.; Joshi, S.; Klappenberger, F.; Samudrala, N.; Barth, J. V. *Nat. Nanotechnol.* **2012**, *7*, 41−46.

(2) Tulevski, G. S.; Miao, Q.; Fukuto, M.; Abram, R.; Ocko, B.; Pindak, R.; Steigerwald, M. L.; Kagan, C. R.; Nuckolls, C. *J. Am. Chem. Soc.* **2004**, *126*, 15048−15050.

(3) Forrest, S. R. *Chem. Rev.* **1997**, *97*, 1793−1896.

(4) Schaer, M.; Nüesch, F.; Berner, D.; Leo, W.; Zuppiroli, L. *Adv. Funct. Mater.* **2001**, *11*, 116−121.

(5) Sasabe, H.; Chiba, T.; Su, S.; Pu, Y.; Nakayama, K.; Kido, J. *Chem. Commun.* **2008**, 5821−5823.

(6) Yokoyama, D.; Sasabe, H.; Furukawa, J.; Adachi, C.; Kido. *J. Adv. Funct. Mater.* **2011**, *21*, 1375−1382.

(7) Williams, F. J.; Vaughan, O. P. H.; Knox, K. J.; Bampos, N.; Lambert, R. M. *Chem. Commun.* **2004**, 1688−1689.

(8) Flechtner, K.; Kretschmann, A.; Steinrück, H.-P.; Gottfried, J. M. *J. Am. Chem. Soc.* **2007**, *129*, 12110−12111.

(9) Flechtner, K.; Kretschmann, A.; Bradshaw, L. R.; Walz, M.-M.; Steinrück, H.-P.; Gottfried, J. M. *J. Phys. Chem. C* **2007**, *111*, 5821−5824.

(10) Katano, S.; Kim, Y.; Hori, M.; Trenary, M.; Kawai, M. *Science* **2007**, *316*, 1883−1886.

(11) Fabris, S.; Stepanow, S.; Lin, N.; Gambardella, P.; Dmitriev, A.; Honolka, J.; Baroni, S.; Kern, K. *Nano Lett.* **2011**, *11*, 5414−5420.

(12) Wintterlin, J.; Völkening, S.; Janssens, T. V. W.; Zambelli, T.; Ertl, G. *Science* **1997**, *278*, 1931−1933.

(13) Matthiesen, J.; Wendt, S.; Hansen, J. Ø.; Madsen, G. K. H.; Lira, E.; Galliker, P.; Vestergaard, E. K.; Schaub, R.; Lægsgaard, E.; Hammer, B.; Besenbacher, F. *ACS Nano* **2009**, *3*, 517−526.
(14) Blake, M. M.; Nanayakkara, S. U.; Claridge, S. A.; Fernandez-Torres, L. C.; Sykes, E. C. H.; Weiss, P. S. *J. Phys. Chem. A* **2009**, *113*, 13167−13172.
(15) Meier, C.; Ziener, U.; Landfester, K.; Weihrich, P. *J. Phys. Chem. B* **2005**, *109*, 21015−21027.
(16) Ziener, U.; Lehn, J. M.; Mourran, A.; Möller, M. *Chem.—Eur. J.* **2002**, *8*, 951.
(17) Hoster, H. E.; Roos, M.; Breitruck, A.; Meier, C.; Tonigold, K.; Waldmann, T.; Ziener, U.; Behm, R. J. *Langmuir* **2007**, *23*, 11570−11579.
(18) Roos, M.; Hoster, H. E.; Breitruck, A.; Behm, R. J. *Phys. Chem. Chem. Phys.* **2007**, *9*, 5672−5679.
(19) Waldmann, T.; Nenon, C.; Hoster, H. E.; Behm, R. J. *Phys. Chem. Chem. Phys.* **2011**, *13*, 20724−20728.
(20) Ling, W. L.; de la Figuera, J.; Bartelt, N. C.; Hwang, R. Q.; Schmid, A. K.; Thayer, G. E.; Hamilton, J. C. *Phys. Rev. Lett.* **2004**, *92*, 116102−1−116102−4.
(21) Angelucci, C. A.; Varela, H.; Herrero, E.; Feliu, J. M. *J. Phys. Chem. C* **2009**, *113*, 18835−18841.
(22) Cheng, Z.; Du, S.; Guo, W.; Gao, L.; Deng, Z.; Jiang, N.; Guo, H.; Tang, H.; Gao, H. *Nano Res.* **2011**, *4*, 523−530.
(23) Carley, A. F.; Davies, P. R.; Edwards, D.; Jones, R. V.; Parsons, M. *Top. Catal.* **2005**, *36*, 21−32.
(24) Davies, P. R.; Shukla, N. *Surf. Sci.* **1995**, *322*, 8−20.
(25) Michaelides, A.; Reuter, K.; Scheffler, M. *J. Vac. Sci. Technol., A* **2005**, *23*, 1487−1497.
(26) Campbell, C. T. *Surf. Sci.* **1985**, *157*, 43−60.
(27) Waldmann, T.; Nenon, C.; Tonigold, K.; Hoster, H. E.; Groß, A.; Behm, R. J. *Phys.Chem.Chem.Phys.* submitted.
(28) Komrowski, A. J.; Sexton, J. Z.; Kummel, A. C. *Phys. Rev. Lett.* **2001**, *87*, 246103−1−246103−4.
(29) Grimme, S.; Antony, J.; Ehrlich, S.; Krieg, H. *J. Chem. Phys.* **2010**, *132*, 154104−154123.
(30) Su, H.-Y.; Yang, M.-M.; Bao, X.-H.; Li, W.-X. *J. of Phys. Chem. C* **2008**, *112*, 17303−17310.
(31) Katritzky, A. R.; Lagowski, J. M. *Chemistry of the Heterocyclic N-Oxides*; Academic Press: New York, 1971.
(32) Becke, A. D. *J. Chem. Phys.* **1993**, *98*, 5648−5652.
(33) McLean, A. D.; Chandler, G. S. *J. Chem. Phys.* **1980**, *72*, 5639−5648.
(34) Frisch, M. J.; Trucks, G. W.; Schlegel, H. B.; Scuseria, G. E.; Robb, M. A.; Cheeseman, J. R.; Montgomery Jr., J. A.; Vreven, T.; Kudin, K. N.; Burant, J. C.; Millam, J. M.; Iyengar, S. S.; Tomasi, J.; Barone, V.; Mennucci, B.; Cossi, M.; Scalmani, G.; Rega, N.; Petersson, G. A.; Nakatsuji, H.; Hada, M.; Ehara, M.; Toyota, K.; Fukuda, R.; Hasegawa, J.; Ishida, M.; Nakajima, T.; Honda, Y.; Kitao, O.; Nakai, H.; Klene, M.; Li, X.; Knox, J. E.; Hratchian, H. P.; Cross, J. B.; Bakken, V.; Adamo, C.; Jaramillo, J.; Gomperts, R.; Stratmann, R. E.; Yazyev, O.; Austin, A. J.; Cammi, R.; Pomelli, C.; Ochterski, J. W.; Ayala, P. Y.; Morokuma, K.; Voth, G. A.; Salvador, P.; Dannenberg, J. J.; Zakrzewski, V. G.; Dapprich, S.; Daniels, A. D.; Strain, M. C.; Farkas, O.; Malick, D. K.; Rabuck, A. D.; Raghavachari, K.; Foresman, J. B.; Ortiz, J. V.; Cui, Q.; Baboul, A. G.; Clifford, S.; Cioslowski, J.; Stefanov, B. B.; Liu, G.; Liashenko, A.; Piskorz, P.; Komaromi, I.; Martin, R. L.; Fox, D. J.; Keith, T.; Al-Laham, M. A.; Peng, C. Y.; Nanayakkara, A.; Challacombe, M.; Gill, P. M. W.; Johnson, B.; Chen, W.; Wong, M. W.; Gonzalez, C.; Pople, J. A. *Gaussian 03*, Revision D.01; Gaussian, Inc.: Wallingford, CT, 2004.
(35) Perdew, J. P.; Burke, K.; Ernzerhof, M. *Phys. Rev. Lett.* **1996**, *77*, 3865−3868.
(36) Kresse, G. *Phys. Rev. B* **1996**, *54*, 11169−11186.
(37) Blöchl, P. E. *Phys. Rev. B* **1994**, *50*, 17953−17979.
(38) Kresse, G.; Joubert, D. *Phys. Rev. B* **1999**, *59*, 1758−1775.
(39) bwGRiD (http://www.bw-grid.de), member of the German D-Grid initiative, funded by the Ministry for Education and Research (Bundesministerium für Bildung and Forschung) and the Ministry for Science, Research and Arts Baden-Württemberg (Ministerium für Wissenschaft, Forschung and Kunst Baden-Württemberg).